JOURNAL OF MATERIALS SCIENCE **37** (2002) 3777 – 3787

Synthesis and characterization of TiBCN coatings deposited by ion beam assisted, co-evaporation electron beam-physical vapor deposition (EB-PVD)

D. E. WOLFE, J. SINGH
Applied Research Laboratory, The Pennsylvania State University, P. O. Box 30, State College, PA 16804, USA
E-mail: dew125@psu.edu

TiC, TiB_2, and super hard TiBCN coatings were successfully deposited by ion beam assisted, electron beam-physical vapor deposition. Titanium, titanium diboride, and carbon (through tungsten) were co-evaporated by energetic electron beams while simultaneously bombarding the substrates with varying ionized gas ratios of nitrogen and argon to obtain super hard TiBCN coatings. The hardness of the TiBCN coating was reported to be equivalent to a soft diamond like carbon film. The adhesion was determined to be greater than 50 N. The hardness, grain size, structure, morphology, crystallographic texture and degree of stress within the coatings were determined using a variety of characterization methods including Vicker's hardness measurements, electron probe microanalysis (EPMA), optical microscopy (OM), scanning electron microscopy (SEM), and X-ray diffraction. The author is not aware of previous TiBCN coatings being deposited by this method.

1. Introduction

First generation coatings primarily consisted of monolithic films of transition metal-carbides and nitrides which aided in improving tool life by several hundred percent [1]. As a result of the need to further improve the hardness and wear resistance of these materials, second generation coatings are presently being explored in which materials with different chemical, physical, tribological, and mechanical functions are being combined in multilayer and nonequilibrium systems including TiBCN. Since most PVD processes are non-equilibrium processes, the inherent coating often contains an increased number of vacancies, grain boundaries, and dislocations as compared to bulk materials. This creates thin film properties that are significantly different from bulk properties. Tailoring thin film properties through materials selection and process optimization has led to significant advancements in coating technology concepts [2–9].

New technology thrusts in tailoring coating design include functionally graded coatings, composite coatings, super hard, metastable multifunctional coatings, nano-crystalline coatings, solid solution coatings, multilayer, and super lattice coatings [10–19]. The coating can be tailored to meet specific material properties. However, knowledge of these material properties must first be identified and understood. Further improvements may even be obtained by combining one or more of the new technology thrusts. In addition to the design of new coating thrusts [9, 10], coating properties are a function of the microstructural features determined by the following processing parameters: deposition temperature, deposition rate, angle of condensation, rotation, method of ion bombardment, ion bombardment densities, energies and types of bombarding species, pressure, substrate surface finish, substrate material, etc., as well as the type of deposition process [17, 18].

Recently, a few authors have explored the deposition of TiBCN coatings by sputtering techniques [20, 21]. Development of super hard, coatings with improved chemical and wear resistance, like TiBCN, will help in further developments in advanced coating materials. However, to date, no one has examined the formation of TiBCN coatings by ion beam assisted, electron beam, physical vapor deposition.

The objective of the present investigation was to synthesize super hard TiBCN coatings by the co-evaporation of titanium, titanium diboride, and carbon (through tungsten) by energetic electron beams while simultaneously bombarding the substrates with varying ionized gas mixtures of nitrogen and argon.

2. Experimental procedure

Coating synthesis was carried out in an industrial prototype Sciaky, Inc. EB-PVD unit consisting of six EB-guns and a three ingot continuous feeding system with ion bombardment capabilities as shown in Fig. 1. The

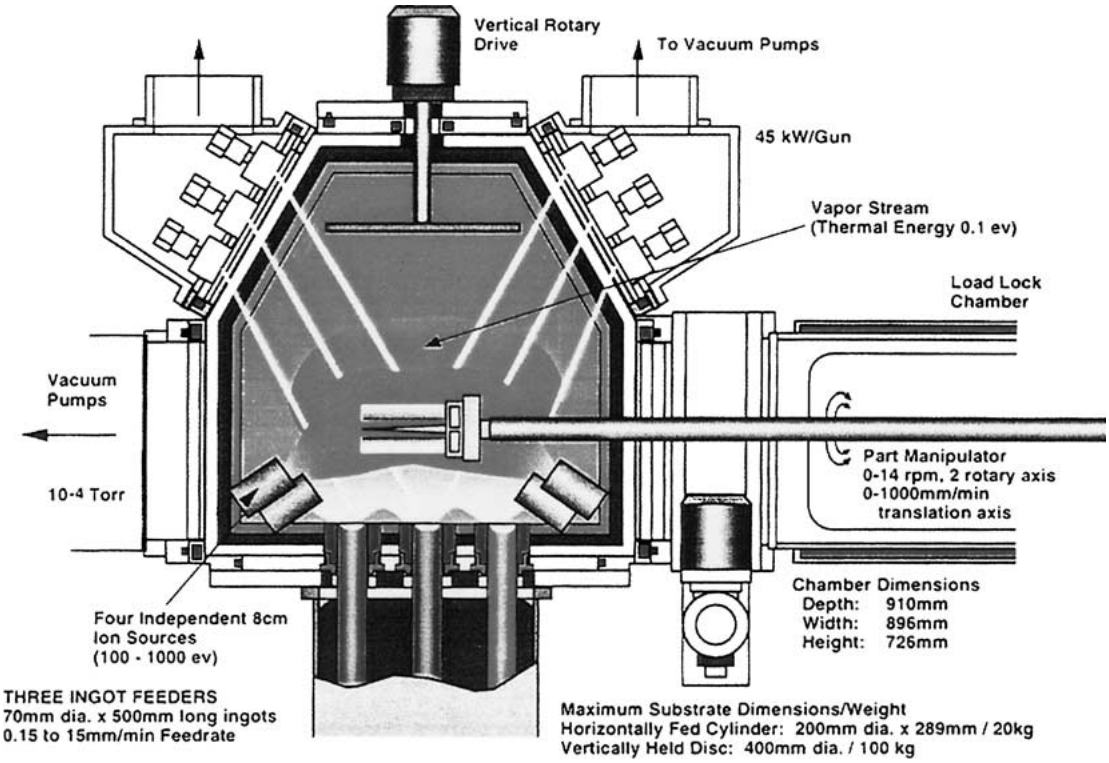

Figure 1 Schematic diagram showing the 6-electron beam gun Sciaky EB-PVD unit used in the formation of TiBCN coatings.

source to substrate distance was 40.64 cm. A mechanical pump evacuated the chamber to $\sim 10^{-3}$ torr, then a diffusion pump evacuated the chamber to approximately $\sim 10^{-6}$ torr. Once the chamber was at a suitable pressure, the substrates were cleaned using argon ion beam sputtering for 90 minutes at 750 V/350 mA.

A 200 V negative d.c. bias was applied to the substrate holder rotating at 40 rpm. The samples (WC-6wt%Co-0.3wt%TaC; style: TPG432) were preheated and allowed to soak at the desired temperature (800°C) for 15 minutes. High purity (99.95%) titanium, carbon and titanium diboride were evaporated by a beam of electrons ~30 degrees from the normal to the surface. During the co-evaporation of Ti, C(W) and TiB_2, the samples were bombarded with a mixture of argon and nitrogen ions (750 eV). The samples were post heated for 15 minutes at the deposition temperature before cooling. Table I lists the deposition parameters for the various coatings.

3. Results and discussion

3.1. Formation of TiBCN and electron probe microanalysis (EPMA)

EPMA was performed on cross sections of the TiBCN coatings to determine the bulk composition. The beam parameters were 15 keV and 20 μA. The standard characteristic wavelengths measured for $Ti_{K\alpha}$, $C_{K\alpha}$, $B_{K\alpha}$, and $N_{K\alpha}$ X-ray lines were obtained from TiC, TiC, TiB_2, and α-Si_3N_4 standards, respectively. Both the samples and standards used in the analysis were gold coated simultaneously by magnetron sputtering to prevent variations of coating thickness. The overlap of the Ti_{L1} on $N_{K\alpha}$ was corrected by measuring the Ti_{L1} intensity at the $N_{K\alpha}$ position on the TiC standard and subtracting the composition dependent intensity during the analysis of the unknowns. Standard ZAF (atomic number (Z), absorption (A), and fluorescence (F)) corrections were made for matrix corrections. $C_{K\alpha}$, $B_{K\alpha}$ and $N_{K\alpha}$ intensities were measured by peak area with

TABLE I Deposition parameters for the formation of TiBCN coatings by the co-evaporation of titanium, titanium diboride, and carbon through tungsten with simultaneous argon/nitrogen bombardment

Sample no.	A	B	C	D	E
Coating description	TiB_2	TiB_2 + Ar	TiBCN	TiBCN	TiBCN
T_{sub} (°C)	800	800	800	800	800
Ar/N_2	0/0	20/0	15/2	30/10	30/20
Evap. rate Ti (g/min.)	0	0	0.284	0.2177	0.288
Evap. rate C (g/min.)	0	0	0.054	0.056	0.058
Evap. rate TiB_2 (g/min.)	0.588	1.07	0.178	1.13	1.09
Deposition time (min)	45	60	70	80	80
Pressure (torr)	$3–4 \times 10^{-4}$	$4–5 \times 10^{-4}$	$3–4 \times 10^{-4}$	$7–8 \times 10^{-4}$	$7–8 \times 10^{-4}$
Ion energy (keV)	N/A	750	750	750	750
Bias (V)	0	−200	−200	−200	−200
Source-substrate (cm)	33.02	40.64	33.02	40.64	40.64

TABLE II EPMA average bulk compositions of the various TiB_2 and TiBCN coatings deposited by ion beam assisted co-evaporation by EB-PVD

Sample number	Ti (at.%)	B (at.%)	C (at.%)	N (at.%)
A	37–40	60–63	N/A	N/A
B	33–34	65–67	N/A	N/A
C	42.54	23.91	24.05	7.08
D	38.90	43.17	13.49	4.45
E	36.01	43.32	12.96	7.71

modeled background. The $Ti_{K\alpha}$ intensity was measured by peak height. Table II lists the bulk composition values determined by EPMA for TiB_2, TiB_2 with argon ion assist, and the three TiBCN samples deposited under varying deposition conditions.

A few percent difference in the concentration of titanium and boron were observed for samples A and B. The difference is attributed to the deposition process. In both cases, TiB_2 material was directly evaporated by electron beams. The main difference between A and B was that B was bombarded with argon ions to change the microstructure and density during deposition. Sample A would suggest that the degree of fractionation of the TiB_2 ingot results in a titanium rich coating. This is typical of the direct evaporation of component material with differing vapor pressures. TiB_2 did not form a conventional melt pool during evaporation. The evaporation can be described more as sublimation. If the processing parameters such as beam size and pattern are not refined, local hot spots in the beam may cause preferential evaporation.

The ideal method of TiB_2 evaporation would be to have a small diameter ingot with the entire surface molten with a constant feed rate. However, having a larger melt pool generally corresponds to higher deposition rates which are not as desirable for wear applications in which the microstructure can significantly influence the properties of the coating. It should be noted that similar behavior was observed where the initial deposition trials of TiB_2 evaporation resulted in coatings that were deficient in boron [20]. Similar to yttria stabilized zirconia evaporation, in which oxygen is backfilled into the chamber to accommodate the oxygen loss resulting from fractionation [18], boron can be introduced into the system by backfilling the chamber with a mixture of hydrogen and boron tetrachloride gases. However, boron tetrachloride is a colorless, odorless, and poisonous gas which causes safety issues. Due to possible dangers involved with using boron tetrachloride gas, it was not performed. Instead, the TiB_2 pool was enriched with boron metal to account for the loss of boron from TiB_2 fractionation. Several trials were performed to determine the feasibility. The results were not promising. In most cases, the boron metal evaporated prior to the TiB_2 forming a thick layer of primarily boron. It was then decided that in order to reduce the effects of fractionation, the electron beam was defocused and rastered over the ingot material. The longitude and frequency values of the deflection pattern were optimized to obtain a near stoichiometric TiB_2 compound. It was anticipated that the loss of boron would make the formation of TiBCN more thermodynamically favorable

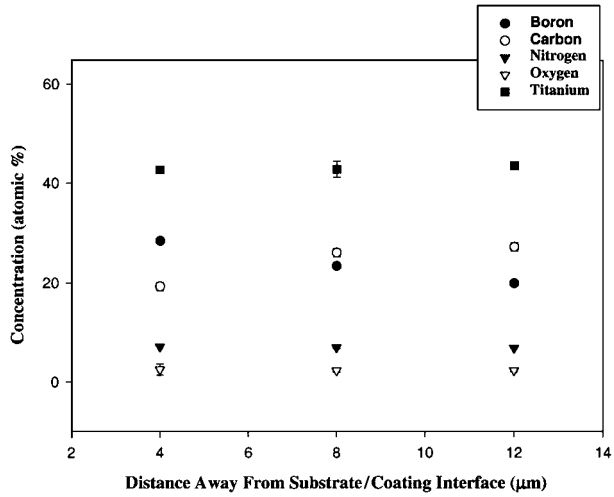

Figure 2 EPMA showing the atomic concentrations of Ti, C, B, N, and O as a function of distance away from the substrate/coating interface for TiBCN coating deposited (sample C) by ion beam assisted, co-evaporation by EB-PVD.

as the strong bonds between the Ti and B would not have to be broken in order to accommodate the carbon and nitrogen atoms.

Prior to the co-evaporation of Ti, C(W) and TiB_2 to form TiBCN, a few experiments were performed to refine the evaporation rates of titanium and carbon through tungsten. The deposition parameters selected resulted in a slightly carbon deficient TiC coating which was desirable to allow the incorporation nitrogen from the ion bombardment of the mixed gas. The composition of sample C showed a nearly equal ratio of boron (230.91 at.%) and carbon (24.05 at.%) with approximately 7.08 at.% nitrogen and 2.415 at.% oxygen. The average atomic % of each constituent element for sample C is plotted as a function of distance away from the substrate/coating interface in Fig. 2. The compositional profile shows a fairly uniform distribution for titanium and nitrogen. The carbon concentration decreases slightly throughout the thickness of the coating whereas the boron concentration increased. This strongly suggests a competition between the carbon and boron incorporation. Another possible explanation is slight changes of the melt pools during deposition which may have contributed to the variation. Further process refinement could produce a more uniform composition.

The deposition conditions were held constant for samples D and E with the exception of the argon/nitrogen ionized gas ratio (30 : 10 and 30 : 20 for samples D and E, respectively). Doubling the nitrogen gas flow into the ion source resulting in an increased nitrogen concentration of almost 75% for sample E without significantly reducing the amount of carbon within the sample (samples D and E). However, the increased nitrogen incorporation (in E as compared to D) resulted in a slight decrease in the titanium concentration. It is believed that the additional nitrogen ions sputtered more titanium atoms from the growing film. Of all the bonds present, the Ti–Ti bond lengths are the largest, and thus the weakest. It should be noted that composition analysis is made very difficult do to the complexity of the elemental composition of the TiBCN coatings

consisting of light elements mixed with a heavy element (titanium).

4. Energy dispersive spectroscopy (EDS)

Energy dispersive spectroscopy was obtained on the surface of the coatings to determine the presence of argon. In all cases (except in the TiB_2 deposited without ion bombardment (sample A)), argon was detected in the coatings. The detection of argon is important in determining possible explanations for the high degree of stress in the deposited coatings which will be discussed in Section 8. Entrapment of gaseous species caused significant amounts of stress in the coating. Without having a standard for comparison, exact determination of the argon concentration is difficult. However, a comparison between the various coatings should yield a qualitative description of the amount of argon incorporated into the coatings from the ion bombardment. The $Ar_{K\alpha 1}$ X-ray line was compared to the $Ti_{K\beta 1}$ x-ray line shown in Fig. 3a–c, for samples A, B, and D, respectively, to determine relative amounts of argon present in the coatings. The EDS spectra for samples C and E were similar to that of Fig. 3c. Several spectra were obtained and averaged to obtain the $Ar_{K\alpha 1}/Ti_{K\beta 1}$. The TiB_2 coating with argon ion assist (sample B) had an $Ar_{K\alpha 1}/Ti_{K\beta 1}$ of 0.88. For comparison, the $Ar_{K\alpha 1}/Ti_{K\beta 1}$ ratios for samples C, D and E (TiBCN) are 0.567, 0.527, and 0.408, respectively. The EDS analysis strongly suggests that large amounts of argon was incorporated into the growing film. This is probably the result of the hexagonal structure of TiB_2 combined with the microstructure of the deposited coating which will be discussed in Section 7. Generally, argon is believed to be incorporated at grain boundaries. Therefore, coatings with smaller grain sizes (i.e., larger number of grain boundaries) would be expected to contain larger amounts of argon. In all three TiBCN samples (C, D, and E), argon incorporation was considerable lower than in the TiB_2 coating deposited with argon ion assist. The lower concentration of argon may be attributed to the increased amounts of nitrogen being incorporated into the coating as well as the structure of the coatings. This appears to be supported by the lower $Ar_{K\alpha 1}/Ti_{K\beta 1}$ for sample E (higher nitrogen concentration) as compared to sample D (lower nitrogen concentration). TiB_2 has a hexagonal structure whereas the TiBCN coatings were cubic as shown by the x-ray diffraction patterns (Section 6). The *c*-axis (0.32295 nm) lattice parameter is larger than the *a*-axis (0.30303 nm) lattice parameter for TiB_2 [22]. The atomic radius of Ar^+ is 0.154 nm which would allow an argon ion to be incorporated between the close packed planes (001) of TiB_2, especially if defects exist such as missing boron atoms. This would suggest some degree of ion channeling discussed in Section 6 concerning the crystallographic texture of the coatings [23].

5. Average Vicker's hardness number (VHN)

The average Vicker's hardness values for the various coated samples are shown in Fig. 4. Direct evaporation of TiB_2 (A) produced a coating hardness of 2356 $VHN_{0.050}$, which is lower than the bulk hardness value of TiB_2 (3200 $VHN_{0.050}$). The low hardness value is most likely the result of the high deposition rate, deviation in stoichiometry and un-refined deposition parameters. During the formation of the TiBCN coatings, the deposition procedures were very complex with 5 electron beam guns operating simultaneously while bombarding the surface with ionized argon and nitrogen gas. As previously discussed, the properties of the coating are a strong function of the deposition technique, as well as deposition parameters. A lower deposition rate should yield a more dense film and thus higher hardness value. Therefore, the low hardness number suggests that the deposition parameters could be optimized to improve the hardness of the coating.

The Vicker's hardness number of the TiB_2 coating increased to 2465 $VHN_{0.050}$ by bombarding the growing film with ionized argon gas during deposition (sample B). The bombarding ions add energy into the system which allows greater surface mobility. This increased surface mobility results in a more dense structure as observed by SEM (Fig. 5d). In addition, the bombarding argon ions force the Ti and B atoms closer together resulting in higher values of compressive stress (Figure 6).

The Vicker's hardness number for the various TiBCN samples ranged from 2777 to 3253 $VHN_{0.050}$. Changing the deposition conditions to incorporate carbon and nitrogen into the condensate to produce a TiBCN (C) coating resulted in an 18% increase in hardness (2777 $VHN_{0.050}$) over the TiB_2 coating alone. The increase is attributed to the complexity

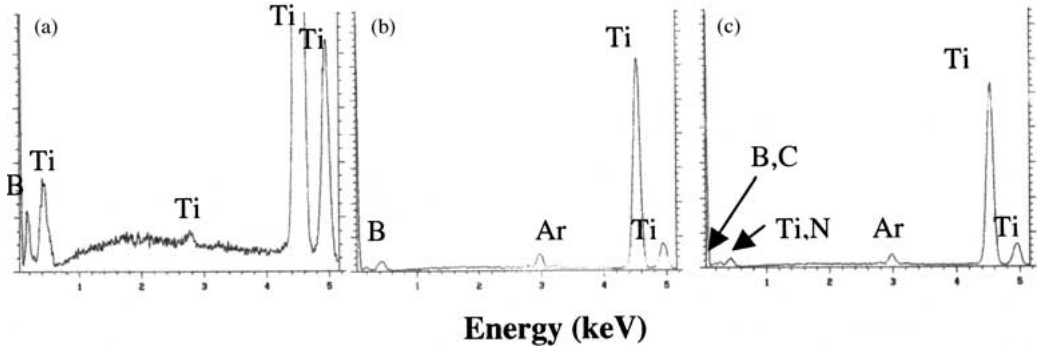

Figure 3 EDS spectrum used in determining the presence of argon incorporation into sample (a) A (TiB_2), (b) B ($TiB_2 + Ar$), (c) C (TiBCN), (d) D (TiBCN), and (e) E (TiBCN) coatings deposited by argon/nitrogen ion beam assisted, co-evaporation by EB-PVD.

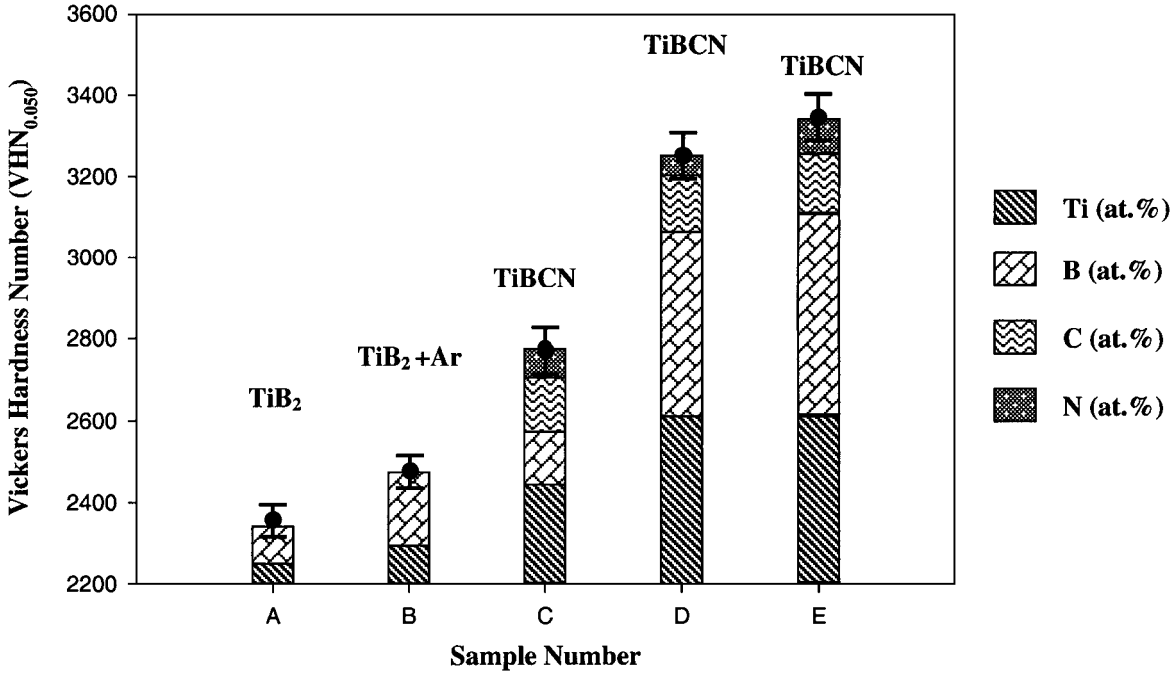

Figure 4 Average Vicker's hardness number ($VHN_{0.050}$) for the various TiB_2 and TiBCN coatings deposited on WC-6wt%Co-0.3wt%TaC by argon/nitrogen ion beam assisted, co-evaporation by EB-PVD.

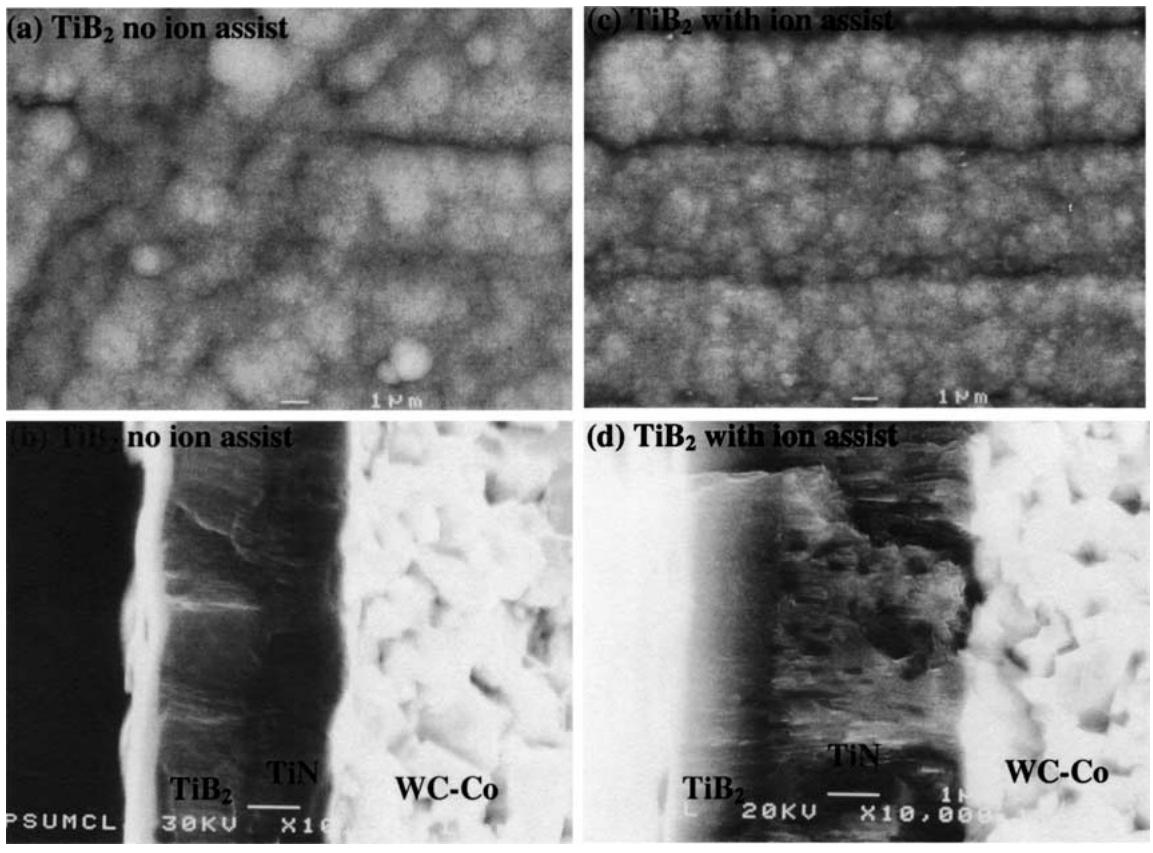

Figure 5 Scanning electron micrographs (SEM) showing the surface morphology and fracture surface of (a, b) TiB_2 deposited without argon ion assist (Sample A) and (c, d) TiB_2 with argon ion assist (Sample B) on a TiN-coated WC-6wt%Co-0.3wt%TaC by EB-PVD.

of the bonding mechanisms resulting from the various elements such as the strong boron-boron bonding combined with the microstructure. A further increase in hardness (over 20%) was obtained by increasing the boron content in the TiBCN coating (sample D (3253 $VHN_{0.050}$)) from 23.91 at.% to 43.173 at.%. Only a 3% further increase in hardness was observed by increasing the nitrogen concentration of the TiBCN coating from 4.448 wt% to 7.712 wt% (E (3343 $VHN_{0.050}$). Several factors can account for the hardness of the deposited coating such as composition, structure, crystallographic texture, microstructure, and stress. However, it is clear that the hardness of the coatings could be further increased by process refinement as well as altering the composition of the TiBCN coatings.

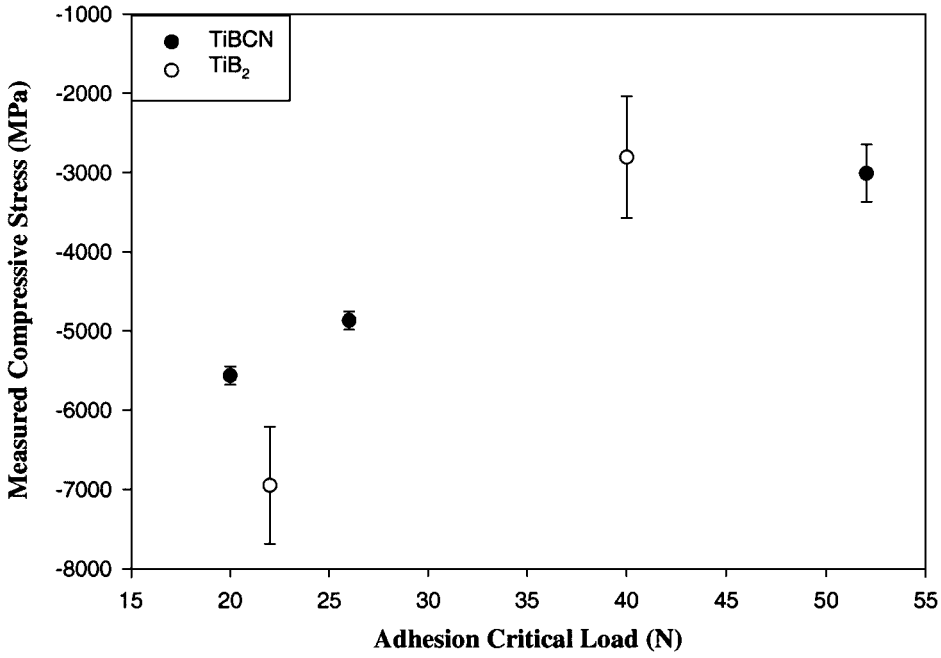

Figure 6 Compressive stress (MPa) as a function of the adhesion critical load for TiBCN and TiB_2 coatings deposited on WC-6wt%Co-0.3wt%TaC by ion beam assisted, co-evaporation by EB-PVD.

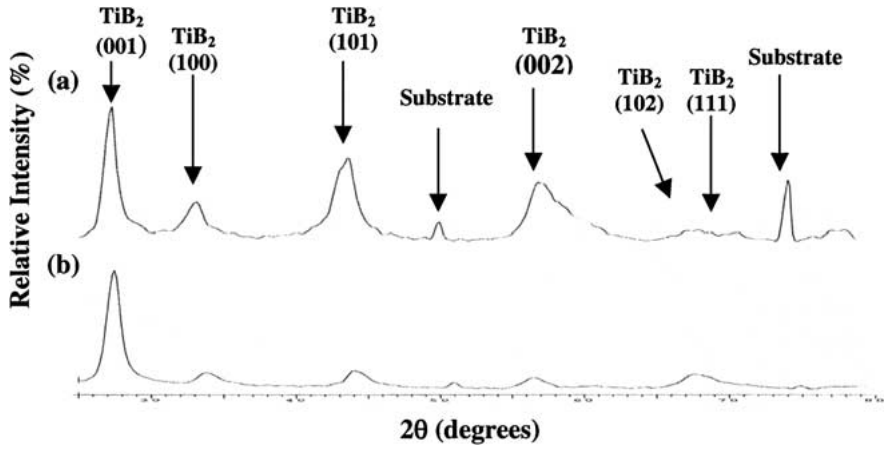

Figure 7 X-ray diffraction pattern of TiB_2 deposited on WC-6wt%Co-0.3wt%TaC by EB-PVD with (a) no argon (Sample A) and (b) argon ion bombardment (Sample B).

6. X-ray diffraction

X-ray diffraction was performed on the samples to determine the structure of the coating. The x-ray diffraction patterns for sample A and B (TiB_2 with and without argon bombardment) are shown in Fig. 7a and b, respectively. The patterns show that the coatings are polycrystalline and of the hexagonal phase (JCPDF #35-741). The lattice parameters for TiB_2 deposited without ion bombardment are $a = 0.3047$ nm and $c = 0.3186$ nm. In comparison, argon bombardment during TiB_2 deposition changed the lattice parameters to $a = 0.3012$ nm and $c = 0.3233$ nm. The standard JCPDF card for hexagonal TiB_2 shows $a = 0.30303$ nm and $c = 0.32295$. The expansion and compression of the a and c axis lattice parameters for sample A, respectively, are most likely the result of stress associated with lattice mismatch and the composition of the coating (Table II). Conversely, the compression and expansion of the a and c lattice parameters for B (argon ion bombardment) may be explained by the forcible incorporation of argon gas. The basal plane is more likely to be compressed, whereas the c lattice parameter is more suitable to accommodate gaseous species and expand. Comparing the relative intensities for the various diffracting planes for the TiB_2 coatings deposited with and without argon ion bombardment, both show a (001) orientation, but the TiB_2 coating deposited with argon bombardment appears to show a much stronger (001) orientation, as the growth of the remaining diffracting planes appears to have been suppressed.

To better quantify the degree of crystallographic texture, the TiB_2 (101) crystallographic texture coefficient was calculated using the following equation:

$$I(101)/(I(101) + I(100))$$

where I is the integrated intensity of the respective diffracting lattice planes. The TiB_2 (101) crystallographic texture coefficient for samples A and B are 0.3846 and 0.1850, respectively. The TiB_2 (101) crystallographic texture coefficient for a randomly oriented sample is 0.64. The additional energy of the system

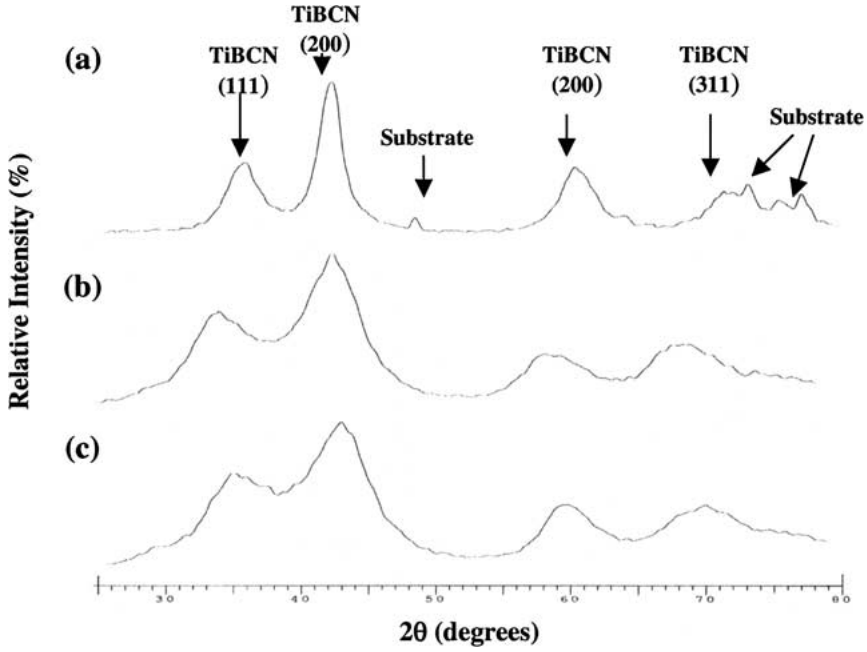

Figure 8 X-ray diffraction pattern of TiBCN deposited on WC-6wt%Co-0.3wt%TaC by co-evaporation using EB-PVD and argon/nitrogen ion bombardment (a) Sample C, (b) Sample D, and (c) Sample E.

resulting from the argon ion bombardment resulted in a stronger (001) orientation. Generally, additional energy to the system will result in changes in crystallographic texture to planes with higher free energy. The ion bombardment allowed the TiB_2 (001) planes to survive which would otherwise not during film growth. The lower TiB_2 (101) crystallographic texture coefficient for sample A supports the presence of argon within the coating. This would also suggest that the mechanism for argon incorporation is ion channeling.

Fig. 8a–c show the x-ray diffraction pattern for samples C-E (TiBCN). The x-ray diffraction patterns for the TiBCN coatings suggest that the coatings are of the cubic phase with a (200) orientation. The lattice parameters were determined to be 0.4365 nm, 0.4410 nm, and 0.4376 nm, respectively, for samples C, D, and E. Since TiBCN is a metastable coating, there is no JCPDF for comparison, which makes confirmation of the coating phase difficult. However, comparing the peak positions and intensities for TiB_2, TiC, and TiN JCPDF cards, it was determined that the diffracting planes matched more closely to the cubic phases of TiC and TiN than to the hexagonal phase of TiB_2. In addition, the large peak broadening strongly suggests that the average crystallite size is relatively small. X-ray diffraction line broadening was used to determine the average crystallite size of the various coatings. Generally, in a single crystal material, sharp distinct peaks are observed for the intensities of the diffracting planes. Broadening (Figs 7 and 8) of these peaks is a function of the average crystallite size and is approximated by the Scherrer formula [24]. Using computer software, the background noise and intensity of Cu $K_{\alpha 2}$ was stripped from the diffraction patterns. The FWHM was determined from the diffracting planes with the three highest intensities for both phases. To eliminate the instrumental error, a silicon single crystal standard was used to determine the x-ray line broadening resulting from the diffractometer. The measured FWHM values were then corrected using the standard before calculating the average crystallite size. The average crystallite size was determined to be 6.6 nm and 12.7 nm for sample A (no IBAD) and B (Ar IBAD), respectively. The increase in the average crystallite size for sample B is attributed to the additional energy of the bombarding argon ions (750 eV). The high-energy of the bombarding argon ions, combined with the high deposition temperature and bias, provided enough energy for the average crystallites to grow as the impacting ions produce localized heat (energy) which leads to coarsening. Other authors have reported this same phenomenon [25]. However, several authors have also reported a reduction in grain size with the use of ion bombardment and was attributed to an increase in local surface defects serving as nucleation sites [26]. Both phenomena (increasing and decreasing grain size) can occur depending on the deposition process and parameters. The average crystallite size for the TiBCN coatings was calculated to be 9.0 nm, 6.7 nm, and 5.9 nm, respectively for samples C-E. It has been reported that more than 5% nitrogen incorporation in TiB_2 would destroy the crystalline structure of the TiB_2 phase resulting in an amorphous structure composed of TiB_2-N [27]. The present investigation confirms that this polycrystalline TiBCN can be synthesized with nitrogen concentrations in excess of 7 atomic %. Again, it should be noted that the deposition technique and processing parameters can greatly influence the coating properties.

Differences in the relative peak positions were also observed in Figs 8a–c (i.e., changes in the lattice parameter) for samples C-E which are attributed to compositional differences and strain within the coatings. This would also suggest that TiBCN exists over a fairly wide compositional range (i.e., $Ti_{0.36-0.42}B_{0.24-0.43}$ $C_{0.13-0.24}$ $N_{0.04-0.08}$) and is most likely a defect structure (with missing atoms on lattice

positions), similar to TiN and TiC. The crystal structure may be similar to TiC and TiN (cubic) in which the light elements (B, C, and N) are substitutional for one another (most likely in combination with one or more vacancies).

7. Scanning electron microscopy (SEM)

7.1. TiB_2 with and without IBAD

SEM analysis of the surface morphology and fracture surface of TiB_2 deposited with and without IBAD is shown in Fig. 5. The TiB_2 coating deposited without argon ion bombardment (sample A) shows an average grain size of approximately of 1–5 μm. Bombarding the surface of the samples while evaporating TiB_2 yielded a slight increase in the grain size (sample B). This corresponds well with the x-ray diffraction line broadening determination of the average crystallite size. The increase in the grain size is attributed to the increased amount of energy associated with the ionized argon atoms. This additional energy, increased the surface mobility of the depositing species resulting in grain growth. As previously mentioned, the larger grain size is the result of the higher energy of the ion source.

For comparison, Fig. 9 shows the surface morphology and fracture surface of a TiB_2 coating deposited without and with argon bombardment on a TiN-coated WC-Co substrate. The average grain size without IBAD is approximately 2 μm and is smaller as a result of the lower deposition temperature (650°C) as compared to Fig. 5a (800°C). The average crystallite size was determined to be ~5 nm. In contrast, Fig. 9c shows the surface of the argon assisted TiB_2 coating in which a much finer grain size is observed, but x-ray diffraction line broadening revealed a larger average crystallite size of ~10.1 nm. This was quite surprising, but can be explained based on the competition between grain growth and nucleation. At the higher substrate temperature (800°C), the additional energy from the ion source (750 eV) resulted in increased surface mobility and thus grain growth, but fewer nucleation sites (Fig. 5a). At lower substrate temperatures (Fig. 9), the deposited atoms have low surface mobility. The increased energy from IBAD was high enough to cause an increase in the number of nucleation sites (resulting in the observed reduced surface grain structure) and high enough to cause the crystallites to grow, but not enough to cause an increase in the surface grain size. This supports competing phenomenon between nucleation and grain growth based on the total energy of the system (i.e., temperature and IBAD). Therefore, the generality of whether ion bombardment increases or decreases grain size, is heavily dependent on the deposition parameters such

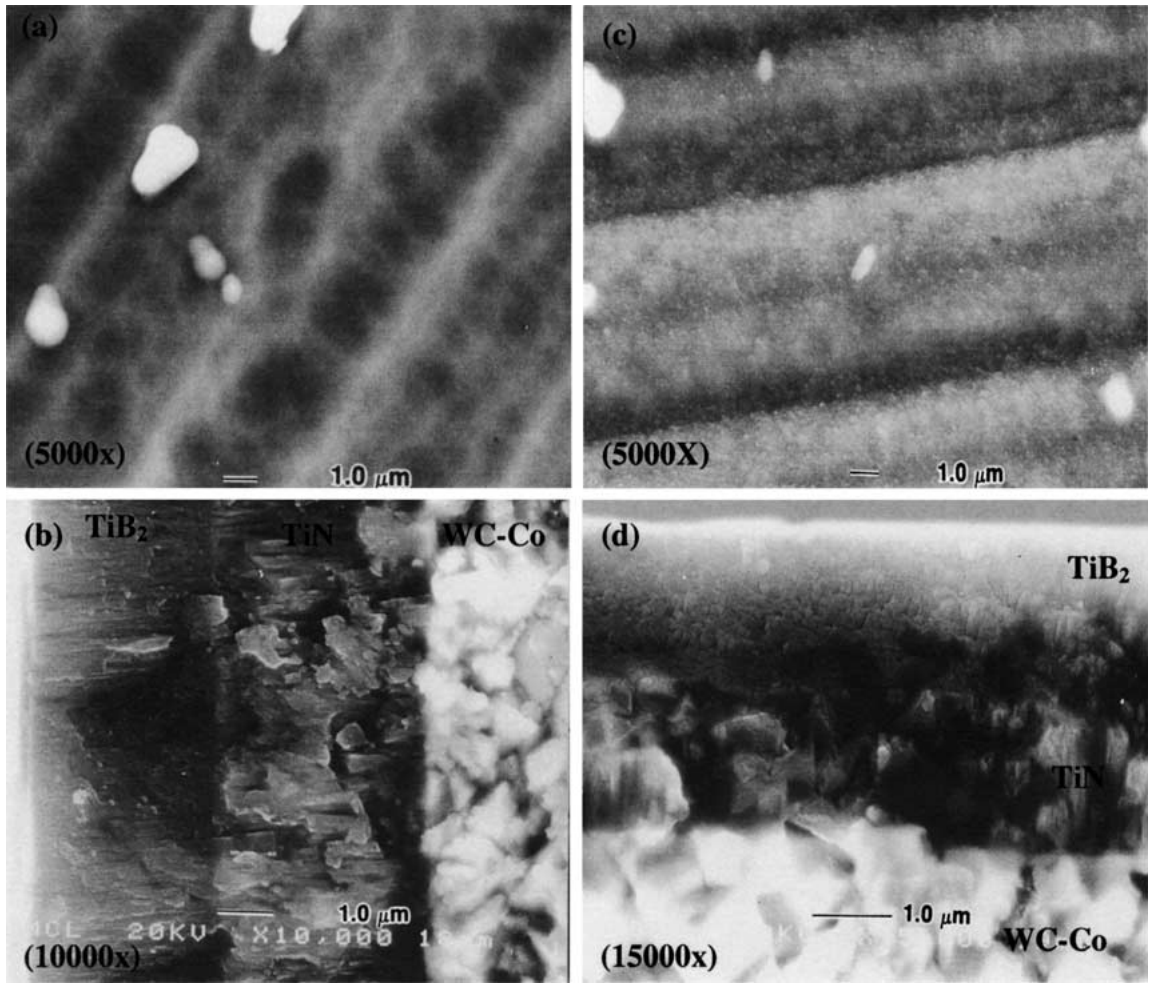

Figure 9 Scanning electron micrographs (SEM) comparing the surface morphology and fracture surface of (a, b) TiB_2 deposited without argon ion assist and (c, d) TiB_2 with argon ion assist on a TiN-coated WC-6wt%Co-0.3wt%TaC by EB-PVD under similar deposition conditions.

as temperature, ion energy, ion current density and deposition parameters.

The fracture surface of the TiB_2 without argon ion assist deposited at low temperature (Fig. 9b) shows a fairly columnar structure whereas the TiB_2 coating deposited at higher substrate temperature (Fig. 5b) shows a more closely packed columnar structure resulting from increased mobility (temperature). In addition, the columnar microstructure of the TiB_2 coating with argon ion assist is barely evident in Fig. 5b, suggesting that it has a much more closely packed structure (ZT or equiaxed) which shows how IBAD can change the microstructure of the coating.

7.2. TiBCN

The microstructures of the TiBCN are difficult to directly compare due to the variations in the deposition parameters resulting from fluctuations during the deposition process. The surface morphology (Fig. 10a) of sample C shows larger grains (~1–5 microns) composed of sub-micron grains > 100 nm in size. No surface cracking was observed in the coating. The larger grains are the result of the underlying substrate surface finish. The grain size is slightly less than sample B. The smaller grain size is attributed to increased incorporation of nitrogen into the growing film which resulted in a lower degree of surface mobility. The increase in the deposited species from the following sources (Ti, TiB_2, and C(W)), resulted in more atoms being depositing without an increase in the amount of ion energy. Therefore, the energy per atom was reduced, resulting in lower surface mobility and thus a smaller grain size. The fracture surface in Fig. 10b shows the titanium layer to be 1.61 μm and the TiBCN (Sample C)

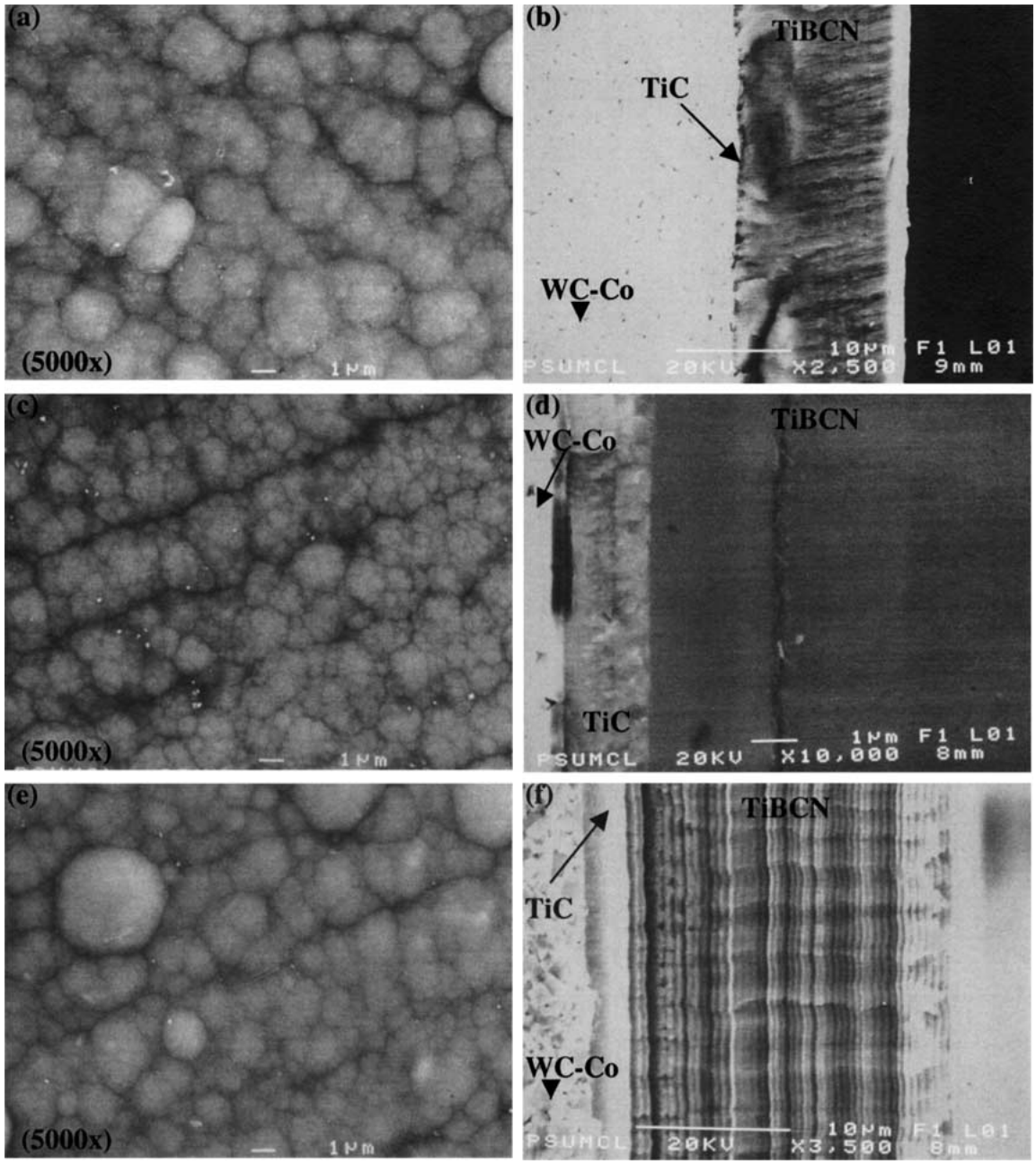

Figure 10 Scanning electron micrographs (SEM) showing the surface morphology and fracture surface of (a, b) Sample C, (c, d) Sample D, and (e, f) Sample E for TiBCN deposited by ion beam assisted, EB-PVD on WC-6wt%Co-0.3wt%TaC.

coating to be 13.22 μm. In addition, Fig. 10b reveals that the TiBCN coating has a columnar structure. Also in Fig. 10b, striations are observed on the micrographs which suggest varying composition or microstructure and discussed in more detail with sample E (Fig. 10f).

Similarly, the surface morphology of sample D (Fig. 10c) shows a fine-grained morphology with a grain size less than 100 nm. The larger grain size for sample D is attributed to the larger coating thickness (25.37 μm) as compared to C (13.22 μm). Fig. 10d shows that the coating consists of a thin layer of titanium (0.3 μm) followed by TiC (1.85 μm) and finally the TiBCN (23.22 μm). The Ti and TiC layers appear to have a columnar structure with the TiBCN being more closely packed. Several process interruptions or fluctuations occurred during the deposition of the TiBCN as is evident by the dark lines in Fig. 10d.

Lastly, Fig. 10e shows the surface morphology of sample E in which a slight reduction in the grain size was observed from sample D. This was unexpected as the coating thickness was comparable (24.52 μm). The reduction in grain size is believed to be associated with the distinct layering observed in Fig. 10f. These layers are much more defined than those observed in Figs 10b and d. The exact cause of the layering is not known, but is believed to be the result of the method of processing (co-evaporation). The periodic arrangement of the layers would suggest that the substrate rotation is a significant contributor to the layers in combination with the orientation of the samples with respect to the source material. However, samples C and D were rotated at the same speed. There is no doubt that the microstructure (and composition) can be refined through process refinement.

8. Stress determination

The stress within the TiBCN and TiB_2 coatings was measured using the $\sin^2\Psi$ technique. The x-ray data was collected using the TiB_2 (101) and the TiBCN (200) planes of the respective coatings. Since the properties of TiBCN are unknown, values for the poisson ratio and Young's modulus similar to titanium carbide were used ($\nu = 0.19$ and E_{200} of 473×10^9 N/m^2) [28]. The TiB_2 coating deposited on WC-6wt%Co-0.3wt%TaC without ion bombardment was determined to be in compression with a value of -2808.5 ± 765 MPa. In contrast, the sample with ion bombardment showed a significant increase in the amount of compressive stress (-6951 ± 739 MPa). The increase in stress is a direct result of argon bombardment in which the high-energy argon atoms (750 eV) cause lattice defects upon impinging on the growing film. The large magnitude of the compressive stress, is the result of the higher energies (750 eV) and current densities ($\sim$0.5 mA/cm^2) used during deposition.

The amount of compressive stress within the TiBCN was found to be very high, but not as high as the TiB_2 coating with argon bombardment. The values were determined to be -3008 ± 361 MPa, -4868 ± 234 MPa, -5562 ± 276 MPa, for samples C, D, and E, respectively. The lower compressive stress for the TiBCN coatings, as compared to the TiB_2 with argon ion assist, is the result of the different ion to atom arrival ratios. During the deposition of sample B ($TiB_2 + Ar$), only TiB_2 ingot was evaporated as compared to Ti, TiB_2, and C(W) for the TiBCN samples. As a result, less energy per atom arrived at the substrate surface as a result of atom collisions within the vapor cloud. During these atom collisions, energy is transferred from atom to atom. Generally, the more collisions an ion undergoes, the less energy it will have when it reaches the surface. In addition, the lower degree of stress may also be associated with the complex interactions between the boron, carbon and nitrogen atoms within the coatings, as well as the lower coating thickness (13.22 μm). Direct comparison of the measured stress values is difficult due to the different compositions of the various coatings as well as the unknown Young's modulus of the material. The differences in the compressive stress values between the various TiBCN coatings may be the result of differences in the composition (as the coating composition can influence the residual stress of a coating) and the varying coating thickness. Lastly, the increase in hardness for sample B (2465 $VHN_{0.050}$) over sample A (2356 $VHN_{0.050}$), cannot be solely related to the amount of compressive stress within the coating. The amount of compressive stress was significantly higher for sample B, but only increased the hardness by a small amount ($<10\%$). This suggests that the dominant mechanism for increased hardness was not stress, but most likely a mixed combination of microstructure and composition. General trends are difficult to state as there the samples were deposited under slightly varying conditions which obviously influenced the microstructure and composition of the coatings.

9. Adhesion

The adhesion of A and B were determined to be 40 and 22 N, respectively, using the scratch test method. The low degree of adhesion for TiB_2 with argon ion assist (B) is attributed to the high degree of compressive stress within the coating (-6951 ± 739 MPa). The adhesion of sample C was found to be $\sim$52 N which had a moderate amount of compressive stress (-3487.4 ± 192 MPa). The low degree of adhesion for samples D (26 N) and E (20 N) are again attributed to a very high degree of compressive stress (-4216.1 ± 199.9 MPa and 4417.6 ± 543.6 MPa, respectively) within the coating. During the scratch test, as shown in Fig. 11 (sample E), cracking was observed prior to adhesive failure. This cracking is most likely the result of the high degree of internal residual stress. The results clearly show that increased amounts of stress within the coating resulted in a reduction of adhesion as shown in Fig. 10. The adhesion of the coatings can be improved by process refinement and possibly using a graded interlayer between the substrate and the TiBCN to reduce the possible stress associated with thermal expansion mismatch.

It should be noted that adhesion tests are generally used for qualitative analysis, but can be used for comparative analysis as the numerical value obtained for the critical adhesion value can vary depending on testing apparatus and environment. Factors which could affect

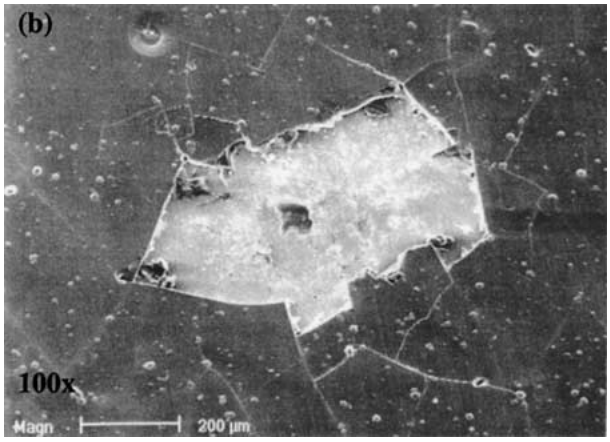

Figure 11 Scanning electron micrographs showing the scratch profile of TiBCN (sample E) deposited on WC-6wt%Co-0.3wt%TaC by EB-PVD.

coating adhesion are: substrate cleaning prior to deposition, interfacial reaction products, test parameters, substrate surface finish, etc.

10. Conclusions

Polycrystalline TiBCN metastable coatings were successfully deposited by the co-evaporation of titanium, titanium diboride, and carbon through tungsten while simultaneously bombarding the surface of the samples with a mixture of argon and nitrogen ionized gas. The composition of the deposited coatings varied considerably, which suggests that the TiBCN is a defect structure which may exist over a wide compositional range similar to TiC and TiB_2. The structure of the TiBCN coating was found to be cubic, which is similar to TiN and TiC phases. Even for the larger concentrations of boron, the phase was still cubic. This is surprising as TiB_2 has a hexagonal structure. The hardness of the TiBCN coatings ranged from 2777 $VHN_{0.050}$ to 3343 $VHN_{0.050}$, showing over a 41% increase over the TiB_2 coating. The highest hardness values were obtained with the coatings with the higher boron content resulting in greater covalent bonding. The adhesion of the TiBCN coatings to WC-6wt%Co-0.3wt%TaC ranged from 20 to 52 N and increased with decreasing stress. Large amounts of compressive stress were found in the coatings resulting from the complex bonding nature of the bonding interactions between carbon, boron, and nitrogen with titanium. Lastly, an increase in the grain size was observed in the TiB_2 coating deposited with ion assist. The increase is do to the additional energy supplied to the system from the high energy ionized argon atoms resulting in coarsening. It should be noted that throughout this investigation, both an increase and decrease in grain size was found with ion bombardment, depending on the processing parameters. This clearly shows the influence of the deposition process on the microstructure of the deposited coatings.

Acknowledgment

This material is based upon work supported by the Department of the Navy Space and Naval Warfare Systems Command under Contract No. N00039-97-D-0042, Delivery Order No. 0215.

References

1. J. E. SUNDGREEN and L. HULTMAN, in Material and Processes for Surface and Interface Engineering, edited by Y. Pauleau (Kluwer Academic Publishers, The Netherlands, 1995) p. 453.
2. B. RAUSHENBACK and K. HELMING, *Nucle. Instrum. Methods. Phys. Res.* B **42** (1989) 216.
3. C. QUAEYHAEGENS, G. KNUYT, J. D'HAEN and L. STALS, *Thin Solid Films* **258** (1995) 170.
4. W. ENSINGER, *Nucle. Instrum. Methods. Phys. Res.* B **106** (1995) 142.
5. G. KNUYT, C. QUAEYHAEGENS, J. D'HAEN and L. STALS, *Thin Solid Films* **258** (1995) 159.
6. U. C. OH and J. H. JE, *J. Appl. Phys.* **74** (1993) 1692.
7. Y. ANDOH, K. OGAA, H. YAMAKI and S. SAKAI, *Nucle. Instrum. Methods. Phys. Res.* B **39** (1989) 158.
8. L. HULTMAN, J. E. SUNGREN, J. E. GREENE, D. N. BERGSTROM and I. PETROV, *J. Appl. Phys.* **78** (1995) 5395.
9. H. HOLLECK and V. SCHIER, *Surface and Coatings Technology* **76/77** (1995) 328.
10. H. HOLLECK, in Surface Engineering: Science and Technology I, edited by A. Kumar *et al.* (The Minerals, Metals and Materials Society, Warrendale, PA, 1999) p. 207.
11. H. DENG, J. CHEN, R. B. INTURI and J. A. BARNARD, *Surface and Coatings Technology* **76/77** (1995) 609.
12. A. KUMAR and M. SHAMSUZZOHA, in Surface Engineering: Science and Technology I, edited by A. Kumar *et al.* (The Minerals, Metals and Materials Society, Warrendale, PA, 1999) p. 165.
13. B. A. MOVCHAN, A. V. DEMCHISHIN, G. G. BADILENKO, R. F. BUNSHAH, C. SANS, C. DESHPANDEY and H. J. DOERR, *Thin Solid Films* **97** (1982) 215.
14. W. ZHANG, B. XU, S. MA, Q. XUE and X. ZHANG, in Surface Engineering: Science and Technology I, edited by A. Kumar *et al.* (The Minerals, Metals and Materials Society, Warrendale, PA, 1999) p. 21.
15. K. J. MA, A. BLOYCE and T. BELL, *Surface and Coatings Technology* **76/77** (1995) 297.
16. D. E. WOLFE and J. SINGH, *ibid.* **124** (2000) 142.
17. *Idem.*, *J. Mater. Sci.* **34** (1999) 2997.
18. *Idem.*, *ibid.* **33** (1998) 3677.
19. H. HOLLECK and M. LAHRES, *Materials Science and Engineering* A **140** (1991) 609.
20. D. E. WOLFE, Thesis 2001dWolfe DE, Penn State University, 2001.
21. D. ZONG, E. SUTTER, J. J. MOORE, G. G. W. MUSTOE, E. A. LEVASHOV and J. DISAM, *Thin Solid Films* **398/399** (2001) 320.
22. M. STUBER, V. SCHIER and H. HOLLECK, *Surface Coatings Technology* **74/75** (1995) 833.
23. W. ENSINGER, *Nucl. Instru. Meth. Phys. Res.* B **106** (1995) 142.
24. B. D. CULLITY, "Elements of X-ray Diffraction" (Addison-Wesley Publishing, Reading, MA, 1978) p. 102.
25. K. BEWILOGUA, H. J. HEINITZ, R. RAU and S. SCHULZE, *Thin Solid Films* **167** (1988) 233.
26. S. K. SHARMA and J. P. MORLEVAT, *ibid.* **156** (1988) 307.
27. T. ARAI and S. MORIYAMA, *ibid.* **259** (1995) 174.
28. A. AUBERT, J. DANROC, A. GAUCHER and J. P. TERRAT, *ibid.* **126** (1985) 61.

Received 19 December 2000
and accepted 17 April 2002